Green Chemistry

ROYAL SOCIETY OF CHEMISTRY

PAPER

View Article Online
View Journal | View Issue

Cite this: *Green Chem.*, 2021, **23**, 3365

Oxo-functionalised mesoionic NHC nickel complexes for selective electrocatalytic reduction of CO_2 to formate†

Simone Bertini, [a] Motiar Rahaman, [a] Abhijit Dutta, [a] Philippe Schollhammer,[b] Alexander V. Rudnev,[a,c] Fredric Gloaguen, *[b] Peter Broekmann *[a] and Martin Albrecht *[a]

Strategies for the conversion of CO_2 to valuable products are paramount for reducing the environmental risks associated with high levels of this greenhouse gas and offer unique opportunities for transforming waste into useful products. While catalysts based on nickel as an Earth-abundant metal for the sustainable reduction of CO_2 are known, the vast majority produce predominantly CO as a product. Here, efficient and selective CO_2 reduction to formate as a synthetically valuable product has been accomplished with novel nickel complexes containing a tailored C,O-bidentate chelating mesoionic carbene ligand. These nickel(II) complexes are easily accessible and show excellent catalytic activity for electrochemical H^+ reduction to H_2 (from HOAc in MeCN), and CO_2 reduction (from CO_2-saturated MeOH/MeCN solution) with high faradaic efficiency to yield formate exclusively as an industrially and synthetically valuable product from CO_2. The most active catalyst precursor features the 4,6-di-*tert*-butyl substituted phenolate triazolylidene ligand, tolerates different proton donors including water, and reaches an unprecedented faradaic efficiency of 83% for formate production, constituting the most active and selective Ni-based system known to date for converting CO_2 into formate as an important commodity chemical.

Received 1st February 2021,
Accepted 12th April 2021

DOI: 10.1039/d1gc00388g

rsc.li/greenchem

Introduction

The conversion of environmentally harmful CO_2 into synthetically and industrially valuable products has become a pressing challenge for mitigating the threats associated with increased CO_2 levels in the atmosphere.[1–3] Among the various technologies developed for CO_2 fixation,[4–6] electrochemical reduction is particularly attractive[7,8] since it allows for direct transformation of CO_2 into synthetically or industrially valuable platform chemicals such as formate,[9,10] alcohols,[11–14] and unsaturated hydrocarbons (*e.g.*, ethylene).[15–17] In addition, electrochemical processes have the benefit to be fully sustainable, especially if they are powered by renewable energy sources (*e.g.*, solar, wind, or hydro). The key critical parameter is then the nature of the catalyst, which is preferably derived from Earth-abundant metals in order to provide a truly sustainable process.[18,19]

While several complexes based on Earth-abundant Mn, Fe, and Ni metals have been known to catalyze the reduction of CO_2,[20–25] the vast majority of these catalysts produce CO as a predominant product.[26,27] Only two Ni systems have been reported to yield formate,[28] namely Sauvage's Ni(cyclam) system from over 30 years ago,[29–32] and Fontecave's Ni(III) catalyst,[33] though selectivity is a major issue in both systems due to significant formation of CO. Formate formation is highly desirable as it constitutes a pathway to convert waste to a valuable product for synthesis, hydrogen storage, formic acid fuel cells, and for other industrial uses.

Inspired by the work of Kirchner and others on manganese pincer complexes,[34–36] which demonstrated a key relevance of the metal-hydride intermediate to promote CO_2 insertion rather than direct CO_2 bonding, we became interested in exploiting the potential of triazolylidenes[37,38] as a specific subclass of N-heterocyclic carbene (NHC) ligands[39–41] for imparting such reactivity. In order to increase the robustness of the

[a]*Department of Chemistry, Biochemistry &Pharmacy, Universität Bern, Freiestrasse 3, 3012 Bern, Switzerland. E-mail: martin.albrecht@dcb.unibe.ch, peter.broekmann@dcb.unibe.ch*
[b]*UMR 6521, CNRS, Université de Bretagne Occidentale, CS 93837, 29238 Brest, France. E-mail: frederic.gloaguen@univ-brest.fr*
[c]*A.N. Frumkin Institute of Physical Chemistry and Electrochemistry Russian Academy of Sciences, Leninskii pr. 31, 119071 Moscow, Russia*

†Electronic supplementary information (ESI) available: Synthesis of all new triazolium salts, NMR spectra and cyclic voltammograms (CVs) of new compounds, NMR and CV experiments in acidic media, details on X-ray diffraction and on electrocatalytic set-up and product identification (PDF), crystallographic data for complexes **3a–c**, **4**, **6a–b** (CIF). CCDC 2004181–2004184, 2050371 and 2050372. For ESI and crystallographic data in CIF or other electronic format see DOI: 10.1039/d1gc00388g

M–C_{NHC} bond and hence the reliability of the carbene as a spectator ligand to the nickel active site,[42] oxygen chelating groups were introduced.[43] Here we show that this approach provides a set of new, tunable, and highly active catalysts for the electrochemical reduction of CO_2 to formate. Catalyst screening in half-cell measurements revealed that the most active system accomplishes unrivalled faradaic efficiency and outstanding selectivity towards formate, largely outperforming currently known catalyst systems based on nickel.

Results and discussion

The new phenolate-substituted triazolium salts **2a–c** were synthesized from 2-azidophenol **1** by [3 + 2] cycloaddition reaction through variation of the alkyne precursor (R = Ph, Bu, Mes; Scheme 1), followed by selective alkylation (>60% overall yield). Metalation was accomplished with $NiCl_2$ as a simple and cheap nickel precursor in the presence of K_2CO_3. The new bis-carbene nickel(II) complexes **3a–c** and **4** were obtained as yellow solids that are stable towards air and moisture for >2 months.

The ^{1}H NMR spectra of the complexes reveal the presence of only one isomer. While complexes **3a**,**b** and **4** feature the phenolate proton resonances in the expected aromatic region (Fig. S20†), the spectrum of complex **3c** is distinct with a markedly upfield shifted phenolate *ortho* proton (δ_H = 4.8; Fig. S20†). This shift of more than 2 ppm suggests a *trans* arrangement of the two *C,O*-bidentate ligands, with the phenolate H_{ortho} influenced by ring current anisotropy of the mesityl group of the other ligand. No such effect has been observed in the NMR spectrum of complex **3b** featuring a phenyl-substituted triazolylidene, which suggests a *cis* configuration. These ligand arrangements were unambiguously confirmed by single crystal X-ray diffraction (Fig. 1). In the trans configuration of **3c**, the mesityl ring is essentially orthogonal to the carbene–Ni plane and close to H_{ortho} (H_{ortho}···arene 2.75 Å), which accounts for the ring anisotropy observed by NMR spectroscopy. The *cis* configuration of the other complexes places the carbene wingtip groups R in close proximity, which results in a substantial distortion from square-planar to tetrahedral (*cf.* $\tau_4 \geq 0.15$).[44] The distortion is larger for bulky wingtip groups (Bu, Ph, in **3a**,**b**, respectively) than with methyl substituents (**4**), and negligible in the *trans* complex **3c** (τ_4 < 0.01; Table S7†).

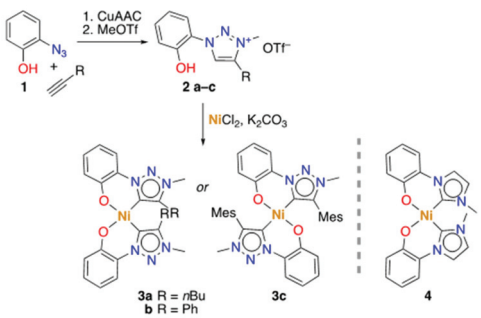

Scheme 1 Synthesis of Ni^{II} bis(carbene) complexes **3** and **4**.

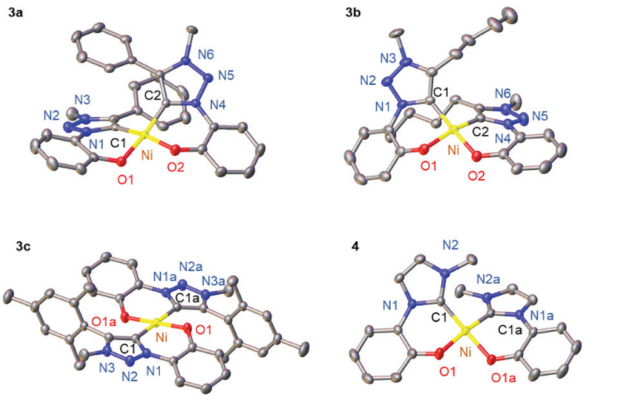

Fig. 1 ORTEP diagram of Ni complexes **3a–c** and **4**; 50% probability level thermal ellipsoids; hydrogen atoms and co-crystallized solvent molecules (H_2O for **3a**, $CHCl_3$ for **4**) omitted for clarity; a denotes symmetry-related atoms.

All four nickel complexes **3a–c**, **4** display (quasi)reversible redox processes around +0.7 V and −2.0 V, tentatively attributed to Ni^{II}/Ni^{III} and Ni^{II}/Ni^{I} transitions, respectively (Fig. 2, S21 and 22;† potentials *vs.* Ag/AgCl).[33] Comparison of the redox potentials consistently indicates that triazolylidenes are stronger donor ligands than imidazolylidene,[45] and that the wingtip group R directly affects the electron density on the nickel center with oxidation potentials increasing along the series R = Bu ($E_{1/2}$ = 0.59) < R = Mes ($E_{1/2}$ = 0.64) < R = Ph ($E_{1/2}$ = 0.69; Table 1).

The electrocatalytic performance of complexes **3a–c**, **4** was first investigated in H^+ reduction. A significant cathodic current was observed when acetic acid (AcOH) was present as proton donor in a MeCN solution of the Ni complex. Increasing the AcOH concentration from 5 to 400 eq. with respect to the Ni complex led to an enhanced current density,

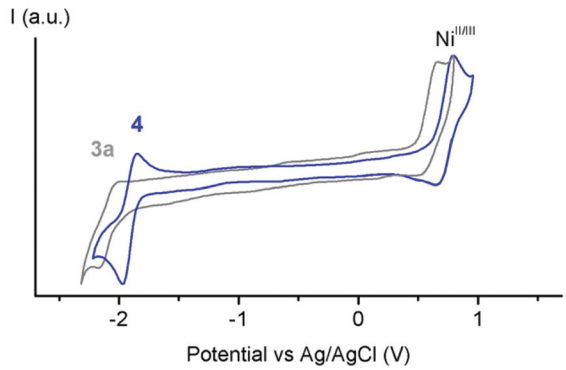

Fig. 2 Cyclic voltammograms of the Ni(II) complexes **3a** (grey) and **4** (blue; both scans 1 mM in MeCN with 0.1 M $(Bu_4N)PF_6$ as supporting electrolyte, 250 mV s^{-1} scan rate, Fc^+/Fc as internal standard with $E_{1/2}$ = 0.36 V *vs.* Ag/AgCl).

Table 1 Redox potentials and catalytic H^+ electroreduction rates for complexes **3** and **4**[a]

Entry	Complex	E_{pc} [b]	$E_{1/2}(Ni^{II/III})$ [b]	k_{obs} [c] [s^{-1}]
1	**3a**	−2.16	0.59 (130)	440
2	**3b**	−2.09	0.69 (110)	300
3	**3c**	−2.12	0.64 (120)	10
4	**4**	−1.92 (110)	0.75 (120)	200

[a] All values in V *vs.* Ag/AgCl; 1 mM MeCN solution of Ni complex with $(Bu_4N)PF_6$ as supporting electrolyte, 250 mV s^{-1} scan rate, Fc^+/Fc as internal standard with $E_{1/2}$ = 0.36 V *vs.* Ag/AgCl. [b] Cathodic peak potential E_{pc} for Ni^{II}/Ni^{I} reduction and half-wave potential $E_{1/2}$ (in parentheses $\Delta E_p = E_{pa} - E_{pc}$ in mV for Ni^{II}/Ni^{III} redox process) [c] Catalytic conditions; 1 mM complex in MeCN, AcOH (0.8 M), $(Bu_4N)PF_6$ as supporting electrolyte, k_{obs} determined by foot of the wave analysis (see ESI for details†).

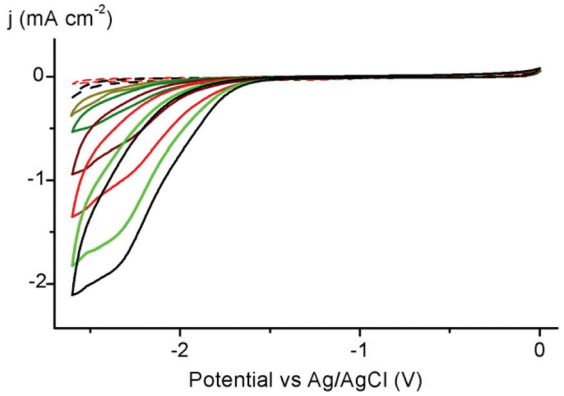

Fig. 3 Electrocatalytic reduction of H^+ in MeCN as solvent (1 mM of complex **3a**, $(Bu_4N)PF_6$ as supporting electrolyte), scan rate 250 mV s^{-1}, HOAc as proton source Fc^+/Fc used as internal standard ($E_{1/2}$ = 0.36 V *vs.* Ag/AgCl); red dashed line: degassed solution of complex **3a** (1 mM) under Ar; black dashed line: degassed solution of AcOH (0.1 M) in MeCN under Ar; olive to black solid lines: complex **3a** (1 mM) in presence of increasing amounts of AcOH (5, 10, 40, 100, 200 and 400 mM, respectively) in MeCN solution).

indicative of catalytic H^+ reduction (Fig. 3). Extraction of k_{obs} by foot-of-the-wave analysis (FOWA)[46,47] reveals a direct influence of the steric and electronic properties of the ligand in promoting catalytic reduction (Table S8†). Specifically, the *trans* arrangement imposed by the very bulky mesityl wingtip groups is strongly deactivating, while all the *cis*-complexes are active. Moreover, the activity of the *cis*-complexes directly correlates with the ligand donor properties deduced from CV data: the alkyl-substituted triazolylidene induces more than a twice higher active than the analogous imidazolylidene (k_{obs} = 440 s^{-1} for **3a** *vs.* 200 s^{-1} for **4**).[48]

Prompted by the promising catalytic activities, complexes **3a–c**, **4** were evaluated as catalyst precursors for electrochemical reduction of CO_2. Initial experiments with a 1 mM MeCN solution of the nickel complex **3a** under a CO_2 atmosphere reveal a significant enhancement of the cathodic current upon complex reduction, indicative of CO_2 transformation (Fig. 4). For complex **4** the reversibility of the Ni^{II}/Ni^{I}

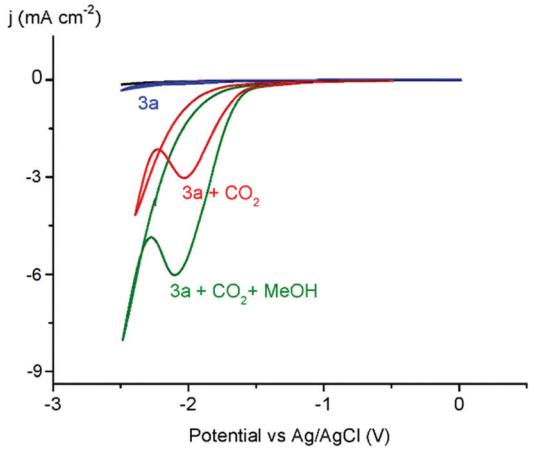

Fig. 4 Electrocatalytic reduction of CO_2 in MeCN with complex **3a** (0.1 M $(Bu_4N)PF_6$ as supporting electrolyte, 250 mV s^{-1} scan rate, glassy carbon working electrode); black line: CO_2-saturated MeCN solution; blue line: degassed solution of complex **3a** (1 mM) under Ar; red line: complex **3a** (1 mM) in CO_2-saturated MeCN solution; green line: complex **3a** (1 mM) in CO_2-saturated MeCN solution with 40 eq. MeOH.

reduction was lost upon saturation with CO_2 gas. All the complexes were active in the process, with only the *trans* isomer **3c** induces low catalytic current, suggesting lower activity. The catalytic current enhances further when the reaction was performed in the presence of MeOH (40 eq. with respect to the Ni complex), suggesting a beneficial role of proton sources.[49] Trifluoroethanol and phenol show similar effects, though the current increase is largest when using MeOH (Fig. 4). Blank measurements indicate no catalytic current with CO_2-saturated solutions in the absence of the Ni complex, or when the complex is reduced in the presence of methanol yet without CO_2 (Fig. S34†).

The robustness of the catalytically active species over time was investigated by chronoamperometry at −1.9 V *vs.* Ag/AgCl in MeOH/MeCN 1 : 50 v : v (Fig. S26–S29†). The observed catalytic current is constant over 2 h, suggesting no significant degradation during that time. More extended reaction reveals a gradual decrease of activity. Comparison of the different complexes reveals catalytic activity for CO_2 reduction follows the same trends observed for H^+ reduction, with highest rates for the nickel complex with the strongest donating triazolylidene ligand (**3a**, k_{obs} = 280 s^{-1}), which is essentially twice as fast as the corresponding imidazolylidene analogue **4** (k_{obs} = 150 s^{-1}; Table 2). Again, the *cis* ligand arrangement is essential for ensuing catalytic activity as the nickel complex **3c** with the ligands in *trans* configuration is almost inactive (k_{obs} = 10 s^{-1}), and enhanced electron density at the nickel center increases catalytic activity (**3a** > **3b** > **4**).

Product identification focused first on gas-phase analysis of volatiles products as most hitherto known Ni catalysts for CO_2 reduction produce CO.[10,11] Remarkably, only traces of H_2 were detected in the gas phase, and CO quantities were below the detection limit (less than 2% faradaic efficiency after 4 h, Table 2). Analysis of the solution phase by ion-exchange

Table 2 Faradaic efficiencies (FE) and catalytic rates for CO_2 conversion with complexes **3a–c** and **4**[a]

Entry	Complex	FE_{HCOO^-} (4 h) [%]	FE_{HCOO^-} (8 h) [%]	FE_{H2+CO} (4 h) [%]	k_{obs}[b] [s^{-1}]
1	**3a**	54	68	3	280
2	**3b**	43	47	4	220
3	**3c**	10	10	2	10
4	**4**	25	25	3	150

[a] General conditions: 1 mM complex, at −1.9 V *vs.* Ag/AgCl, glassy carbon working electrode and Pt foil as counter electrode (see ESI for details†) in MeOH/MeCN 1 : 50 v : v with 0.1 M $(Bu_4N)PF_6$ as supporting electrolyte. [b] Determined from foot of the wave data treatment (see ESI for details†).

chromatography (IC), HPLC and NMR measurements identified formate as the principal product of CO_2 reduction with complexes **3a–c**, **4**. Complex **3a** does not display only the highest activity but also imparts the highest selectivity. Optimization of reaction times affords faradaic efficiencies up to 70% for formate formation, one of the highest known so far for homogeneous Ni-based electrocatalysts.[10,11]

Ligand tailoring has been used to further improve the catalytic activity of these nickel complexes, in particular through introduction of electron-donating substituents on the phenolate. Substitution of the 4,6-positions moreover avoids undesired radical reactions of the phenolate, which may infer from one-electron-reduction upon catalyst activation. To this end the 4,6-Me_2-phenol-triazolium salt **5a** was nickelated *via* the procedure established for the synthesis of **3a**, while the *t*Bu analogue **5b** required *n*BuLi as a stronger base to accomplish nickel complexation (Fig. 5a). The new *O,C*-bidentate chelated trz Ni(II) complexes **6a** and **6b** showed NMR characteristic reminiscent of those of **3a,b**, indicating the formation of the *cis*-isomers exclusively. This structural assignment was further

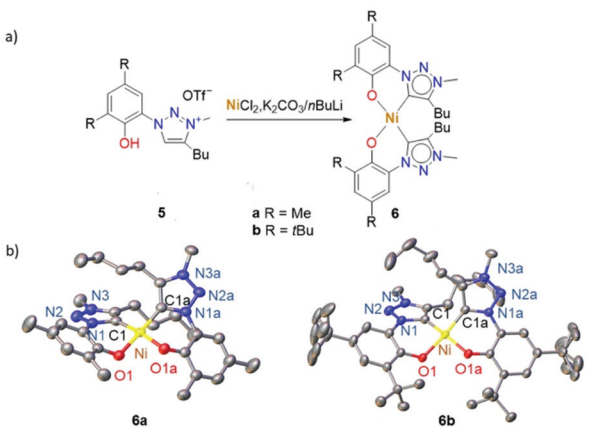

Fig. 5 (a) Synthesis of complexes **6a,b**; (b) ORTEP diagrams of Ni complexes **6a,b** (50% probability thermal ellipsoids, hydrogen atoms omitted for clarity, a denotes symmetry-related atoms). One *t*Bu group in **6b** is disordered about 2 conformations. Selected bond lengths (Å) for **6a**: Ni–C1 = 1.862(2), Ni–O1 = 1.887(1). Selected bond lengths (Å) for **6b**: Ni–C1 = 1.836(1), Ni–O1 = 1.899(1).

confirmed by single crystal X-ray diffraction studies of complexes **6a,b** (Fig. 5b). The distortion from square planar geometry in these complexes is slightly less than in the parent complex **3a** with τ_4 values of 0.15 and 0.18 for **6a** and **6b**, respectively (*cf.* 0.21 for **3a**, Table S7†).

The electrochemical properties of complexes **6a,b** are comparable to those of complexes **3a–c**, featuring a quasi-reversible oxidation at 0.49 and 0.45 V *vs.* Ag/AgCl, respectively, and an irreversible reduction below −2.0 V (Fig. S21 and 22†). The incorporation of donating groups on the phenolate lowers the redox potentials by about 90 (R = Me, **6a**) and 150 mV (R = *t*Bu, **6b** relative to the parent phenolate complex **3a** (Table 3). These potential shifts indicate enhanced electron density at the metal center and efficient electronic tailoring of the nickel center by ligand modifications.

In these *cis* triazolylidene Ni complexes, lower reduction potentials are correlated with higher electrocatalytic CO_2 reduction activity (*cf.* Table 2) Indeed, the stronger donor ligands in complexes **6a,b** and the associated low reduction potential improved the catalytic performance. Foot of the wave data analysis revealed a higher k_{obs} for CO_2 reduction for **6a** than for the parent complex **3a** (300 *vs.* 280 s^{-1}; Table 3), and more significantly for **6b** with the lowest reduction potential (k_{obs} = 370 s^{-1}). Moreover, the robustness of the catalytically active species is demonstrated by a constant catalytic current over the first 2 h (Fig. 6 and S31†). Formate was identified as exclusive product of CO_2 reduction also with complexes **6a,b** with only traces of H_2 and CO as side products. Complex **6b** revealed the highest FE of 83% for formate formation and represents a new benchmark for Ni in this transformation. Moreover, these results demonstrate that ligand tailoring on a molecular level through incorporation of electron-donating substituents provides an efficient strategy for catalyst optimization for this CO_2 reduction and leads in this case to a marked increase of the FE to unprecedented 83%.

While this work is focused on catalyst optimization for the CO_2 reduction half-reaction, obviously also the availability of protons is elementary as the efficiency of the CO_2 to formate transformation is associated with a coupled electron/proton transfer. Variation of the proton source has been accomplished

Table 3 Faradaic efficiencies (FE) and catalytic rates for CO_2 conversion with complexes **6a,b**[a]

Entry	Complex	E_{pc}[b] [V]	FE_{HCOO^-} (8 h) [%]	FE_{H2+CO} (4 h) [%]	k_{obs}[c] [s^{-1}]
1	**6a**	−2.23	74	4	300
2	**6b**	−2.31	83	3	370

[a] General conditions: 1 mM complex, at −1.9 V *vs.* Ag/AgCl, glassy carbon working electrode and Pt foil as counter electrode (see ESI for details†) in MeOH/MeCN 1 : 50 v : v with 0.1 M $(Bu_4N)PF_6$ as supporting electrolyte. [b] Cathodic peak potential E_{pc} for Ni^{II}/Ni^{I} reduction in V *vs.* Ag/AgCl; 1 mM MeCN solution of Ni complex with $(Bu_4N)PF_6$ as supporting electrolyte, 250 mV s^{-1} scan rate, Fc^+/Fc as internal standard with $E_{1/2}$ = 0.36 V *vs.* Ag/AgCl. [c] Determined from foot of the wave data treatment (see ESI for details†).

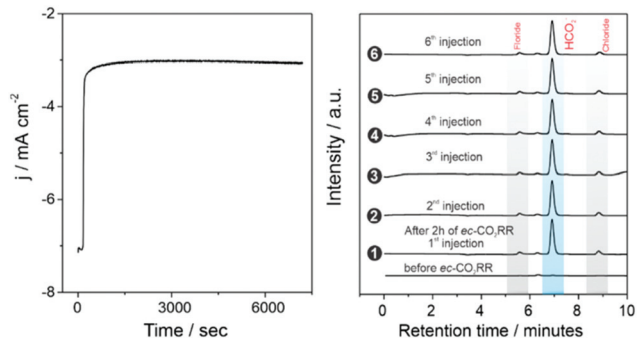

Fig. 6 Electrolysis experiment performed with 1 mM complex **6b**, at −1.9 V *vs.* Ag/AgCl, using glassy carbon working electrode, in a CO_2 saturated solution of MeOH/MeCN 1 : 50 v : v with 0.1 M $(Bu_4N)PF_6$ as supporting electrolyte (left) and product analysis data on six different injections after 2 h by ion exchange chromatography (right).

by varying the additive to the aprotic solvent (MeCN) from MeOH to different proton donors including PhOH, iPrOH, CF_3CH_2OH (TFE), and H_2O (Fig. 7 and S32†). All these proton sources are mediating CO_2 reduction, yet with variable efficiency. Notably, water as the cleanest proton source is tolerated and affords considerable yields of formic acid. Best performance was achieved with TFE, reaching FEs up to 82% within 2 h. These data indicate that formate is exclusively formed at the cathode and not anodically, *e.g.* by partial MeOH oxidation, and that MeOH is not required to achieve high formate yields. Moreover, the broad tolerance of a variety of proton sources provides ample opportunities for optimizing also the oxidation half-reaction for designing an efficient full cell electrolyzer.

Total FE values below 100% suggest parasitic side reactions and catalyst deactivation, which might be triggered by several factors, including acidification of the reaction medium due to the generated formate, (*cf.* H^+ reduction with high HOAc concentrations above). This limitation should be easily mitigated,

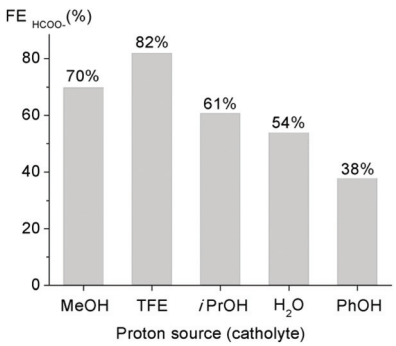

Fig. 7 Comparison of the faradaic efficiencies (FE) for formate in a CO_2-saturated solution containing 1 mM complex **6b** with 0.5 M of different proton donors (in MeCN containing 0.1 M $(Bu_4N)PF_6$ as supporting electrolyte). Electrocatalytic CO_2 reduction was performed at −1.9 V *vs.* Ag/AgCl for 2 h using glassy carbon working electrode; the formate yield was quantified by ion exchange chromatography (Fig. S32†).

for example, by using a flow reactor. Catalyst deactivation during CO_2 electroreduction was evidenced by a combination of high-resolution scanning electron microscopy (HR-SEM), energy dispersive X-ray spectroscopy (EDX) and X-ray diffraction (XRD) analyses with an electrode containing complex **6b** after 2 h of operation at −1.9 V *vs.* Ag/AgCl. Post-electrolytic HR-SEM and XRD analyses identified Ni oxide nanoparticles on the working electrode surface, while EDX suggests formation of films that are too thin for detection (Fig. S37†). Specifically, XRD revealed trace 2θ intensities that are characteristic of NiO and Ni_2O_3 on the electrode surface (Fig. S38†). Nickel oxide formation may be rationalized by partial reduction of the complexed nickel to Ni^0 under the cathodic potential applied during electrolysis, which induces complex decomposition and formation of Ni nanoparticles. These electrochemically generated Ni nanoparticles were probably transformed to Ni oxides (NiO/Ni_2O_3) only when the electrode was exposed to air after the experiment. Such partial complex degradation thus provides a plausible rationale for the gradual loss of activity during extended reaction times and may account for the uncompensated charge from chronoamperometric experiments as some cathodic charge is involved in the *in situ* reduction of Ni^{n+} to Ni^0 during the CO_2 reduction process. It must be noted, however, that Ni nanoparticles are unable to catalyze CO_2 reduction and only induce H_2 formation (HER), independent of size and shape of these nanoparticles.[50] Therefore the highly selective reduction of CO_2 to formate as observed here is confidently attributed to the distinct catalytic activity of the molecularly defined NHC Ni complexes.

The production of formate as valuable product from CO_2 reduction is very rare for nickel-based catalysts, as most Ni systems produce CO.[9] The best complex of the series, complex **6b** shows high faradaic efficiency and exquisite formate *vs.* CO selectivity. The two other known Ni systems generating formate are less efficient in comparison and produce considerable amounts of CO as by-product (Table S11†).[10,11] The triazolylidene system presented here offers unique potential, due to the intrinsically high selectivity towards formate production, and because the catalytic rate can be further optimized due to the correlation of rational ligand design and reduction potentials with catalytic activity. Moreover, a variety of proton sources are tolerated, including water. The largest drawback is probably the high overpotential required in comparison to the Kubiak-Sauvage electrocatalyst (ΔE = 0.5 V).[11]

The poor catalytic activity of the trans isomer points to a key role of the complex geometry. Either, the distortion from square-planar in the *cis* complexes may facilitate the formation of a penta-coordinate nickel(I) intermediate, or more likely, the *cis*-arrangement of the two oxygen donors produces a proton acceptor pocket, especially after one-electron reduction to either a formal nickel(I) complex or a phenoxide radical anion.[51,52] Proton chelation by the two oxygen units is therefore suggested to form the reduced complex **A** (Scheme 2), presumably through a proton-coupled electron transfer (PCET). This intermediate facilitates the formation of a nickel(III)

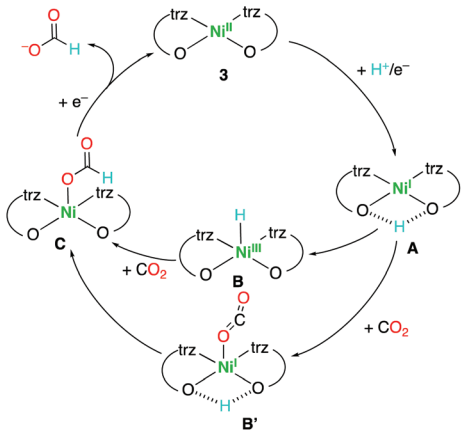

Scheme 2 Proposed mechanism for CO_2 electroreduction with complexes **3** (and **6**).

hydride intermediate **B** for CO_2 insertion and generation of the formate complex **C**, which is then readily reduced to release the formate product. Formation of the nickel hydride intermediate is presumed to be key for the product selectivity,[34–36,53–55] as most known nickel catalysts for CO_2 reduction bind CO_2 directly and therefore produce CO rather than formate.[20,29–32,54–59] Alternatively, the proton scavenging may localize the negative charge on the oxygen, which facilitates the formation of the η1–OCO Ni adduct **B′** as another potentially critical intermediate for formate formation.[60] Attempts to characterize the putative nickel(I) intermediate by spectroelectrochemistry were not successful, as a solution of complex **3a** or **4** did not produce any EPR signal after electrolysis at −2.0 V *vs*. Ag/AgCl, presumably because the nickel(I) species is not sufficiently stable in the absence of substrates. Nonetheless, this mechanistic proposal provides a rationale for the strong divergence of catalytic activity of the *cis vs*. trans complexes.

Conclusions

In summary, we have synthesized and characterized a new class of bis-carbene nickel(II) complexes containing *C,O*-bidentate chelating phenolate-NHC ligands. These complexes are active in the selective electroreduction of CO_2 to formate, reaching up to 83% faradaic efficiency, which is the highest value reported for a Ni-based electrocatalyst to date. Tailoring of the complexes substantially affects activity, with the *cis* isomers outperforming the trans analogue and a more nucleophilic nickel center achieving higher activities. The exquisite selectivity towards formate combined with the tolerance of a variety of proton sources hold great promises for optimizing also the anodic half-reaction and to develop a whole cell system for process operation. The unique aspects of this new class of complexes together with the viability of ligand modification, will provide new perspectives towards the design of novel electrocatalytic systems suitable for small molecules activation.

Experimental section

General

2-Azidophenol 1, 1-(2-phenol)-imidazole 7 and 2-amino-4,6-ditertbutylphenol were synthesized following procedures reported in literature.[61–63] The synthesis of all triazolium salt ligand precursors (**2a–c**, **5a–b**) is detailed in the ESI.† All other reagents were commercially available and used as received. Unless specified otherwise, NMR spectra were recorded at 25 °C with Bruker spectrometers operating at 300 or 400 MHz (^{1}H NMR), and 100 MHz (^{13}C NMR), respectively. Chemical shifts (δ in ppm, coupling constants J in Hz) were referenced to residual solvent signals (^{1}H, ^{13}C). Assignments are based on homo– and heteronuclear shift correlation spectroscopy. The purity of bulk samples of the complexes has been established by NMR spectroscopy, and by elemental analysis, which were performed at the University of Bern Microanalytic Laboratory by using a Thermo Scientific Flash 2000 CHNS–O elemental analyzer. Residual solvent was confirmed by NMR spectroscopy and also by X–ray structure determinations. High–resolution mass spectrometry was carried out with a Thermo Scientific LTQ Orbitrap XL (ESI–TOF).

General procedure for synthesis of the nickel complexes 3a–c, 4 and 6a

The triazolium salt (0.5 mmol), K_2CO_3 (1 mmol) and $NiCl_2$ (0.3 mmol) were suspended in dry MeCN under N_2 atmosphere. The mixture was stirred at reflux temperature for 16 h and filtered through Celite (5 g). The filtrate was evaporated to dryness and the residue was extracted with CH_2Cl_2 and dried *in vacuo*. The residual powder was purified by column chromatography (Al_2O_3 basic; CH_3CN/CH_2Cl_2 1 : 1). Single crystals suitable for X-ray diffraction analysis were obtained by slow diffusion of pentane into a CH_2Cl_2 solution of the complex.

Synthesis of *cis*-[Ni(trz^{Bu}^OPh)$_2$] (3a)

According to the general procedure, reaction of **2a** (200 mg, 0.52 mmol), $NiCl_2$ (44 mg, 0.3 mmol), and K_2CO_3 (140 mg, 1 mmol) in MeCN (10 mL) afford **3a** as a yellow crystalline powder (90 mg, 66%). ^{1}H NMR (400 MHz, CD_2Cl_2): δ 7.68 (d, J = 8.2 Hz, 1H, H_{PhO}), 7.14 (t, J = 8.2 Hz, 1H, H_{PhO}), 7.01 (d, J = 8.2 Hz, 1H, H_{PhO}), 6.56 (t, J = 8.2 Hz, 1H, H_{PhO}), 3.98 (s, 3H, CH_3–N), 2.40–2.22 (m, 1H, $C_{trz}CH_2$), 2.03–1.83 (m, 2H, $C_{trz}CH_2CH_2$), 1.58–1.41 (m, 1H, $C_{trz}CH_2$), 1.38–1.17 (m, 2H, CH_2CH_3), 0.73 (t, J = 6.5 Hz, 3H, CH_3). ^{13}C{^{1}H} NMR (101 MHz, CD_2Cl_2): δ 159.92 (C–O), 146.40 (C_{trz}–Bu), 141.66 (C_{trz}–Ni), 129.73 (C_{PhO}–N), 127.41 (C_{PhO}–H), 122.35 (C_{PhO}–H), 119.60 (C_{PhO}–H), 113.16 (C_{PhO}–H), 36.44 (CH_3–N), 31.97 ($C_{trz}CH_2$), 24.85 ($C_{trz}CH_2CH_2$), 22.78 (CH_2CH_3), 13.53 (CH_3). HR-MS (ESI): calcd for $C_{26}H_{32}O_2N_6Ni$ $[M + Na]^+$ m/z = 518.1935 (found 518.1916). Anal. calcd for $C_{26}H_{32}O_2N_6Ni$ (519.28) × 0.5%

CH_2Cl_2: C, 56.34; H, 5.89; N, 14.85. Found: C, 56.33; H, 5.67; N, 14.74.

Synthesis of *cis*-[Ni(trz^{Ph}^OPh)$_2$] (3b)

According to the general procedure starting from **2b** (200 mg, 0.50 mmol), $NiCl_2$ (42 mg, 0.3 mmol), and K_2CO_3 (140 mg, 1 mmol) in MeCN (10 mL) afforded complex **3b** as a yellow crystalline powder (108 mg, 77%). ^{1}H NMR (400 MHz, CD_2Cl_2): δ 7.70 (d, J = 8.5 Hz, 2H, H_{Ph}), 7.58 (d, J = 8.5 Hz, 1H, H_{PhO}), 7.32–7.25 (m, 3H, H_{Ph}), 7.20 (d, J = 8.5 Hz, 1H, H_{PhO}), 7.10 (t, J = 8.5 Hz, 1H, H_{PhO}), 6.60 (t, J = 8.5 Hz, 1H, H_{PhO}), 3.7 (s, 3H, N–CH_3). $^{13}C\{^1H\}$ NMR (101 MHz, CD_2Cl_2): δ 159.37 (C–O), 145.07 (C_{trz}–Ph), 144.41 (C_{trz}–Ni), 130.15 (C_{Ph}–H), 129.67 (C_{Ph}–H), 129.40 (C_{PhO}–N), 127.44 (C_{Ph}–H), 127.11 (C_{PhO}–H), 126.88 (C_{Ph}–Trz), 122.70 (C_{PhO}–H), 119.29 (C_{PhO}–H), 113.55 (C_{PhO}–H), 37.28 (N–CH_3). HR-MS (ESI): calcd for $C_{30}H_{24}N_6NiO_2$ $[M + Na]^+$ m/z = 581.1206 (found 581.1205). Anal. calcd for $C_{30}H_{24}N_6NiO_2$ (559.26): C, 64.43; H, 4.33; N, 15.03. Found: C, 64.29; H, 4.08; N, 15.15.

Synthesis of *trans*-[Ni(trz^{Mes}^OPh)$_2$] (3c)

The reaction of triazolium salt **2c** (200 mg, 0.45 mmol), $NiCl_2$ (44 mg, 0.34 mmol) and K_2CO_3 (124 mg, 0.9 mmol) in MeCN (10 mL) according to the general procedure yielded complex **3c** as a yellow crystalline powder (51 mg, 35%). ^{1}H NMR (400 MHz, CD_2Cl_2): δ 7.80 (d, J = 8.5 Hz, 1H, H_{PhO}), 7.02 (s, 2H, H_{Mes}), 6.64 (t, J = 8.5 Hz, 1H, H_{PhO}), 6.35 (t, J = 8.5 Hz, 1H, H_{PhO}), 4.97 (d, J = 8.5 Hz 1H, H_{PhO}), 3.67 (s, 3H, CH_3–N), 2.39 (s, 3H, CH_3–Mes), 2.25 (s, 6H, CH_3–Mes). $^{13}C\{^1H\}$ NMR (101 MHz, CD_2Cl_2): δ 157.79 (C–O), 148.98 (C_{PhO}–H), 144.33 (C_{trz}–Mes), 138.72 (C_{trz}–Ni), 137.93 (C_{PhO}-N), 128.40 (C_{Mes}–H), 127.59 (C_{PhO}–H), 127.343 (C_{Mes}–CH_3), 125.79 (C_{PhO}–H), 122.91 (C_{trz}–Mes), 118.23 (C_{PhO}–H), 112.71 (C_{Mes}–CH_3), 35.32 (CH_3–N), 21.02 (CH_3–Mes), 20.32 (CH_3–Mes). HR-MS (ESI): calcd for $C_{36}H_{36}N_6NaNiO_2$ $[M + Na]^+$ m/z = 665.2130 (found 665.2145). Anal. calcd for $C_{36}H_{36}N_6NiO_2$ (643.42): C, 67.20; H, 5.64; N, 13.06. Found: C, 67.00; H, 5.98; N, 12.95.

Synthesis of *cis*-[Ni(imi^{Me}^OPh)$_2$] (4)

According to the general procedure, reaction of 1-(2-phenol)-3-methyl-imidazolium iodide **9** (200 mg, 0.61 mmol), $NiCl_2$ (42 mg, 0.3 mmol), and K_2CO_3 (200 mg, 1.4 mmol) in MeCN (10 mL) and purification by column chromatography (Al_2O_3; CH_3CN/CH_2Cl_2 1 : 2) gave complex **4** as a yellow crystalline powder (90 mg, 70%). ^{1}H NMR (400 MHz, CD_2Cl_2): δ 7.33–7.12 (m, 3H, $2H_{PhO}$ + $1H_{imi}$), 7.03 (t, J = 8.5 Hz, 1H, H_{PhO}), 6.92 (s, 1H, H_{imi}), 6.61 (t, J = 8.5 Hz, 1H, H_{PhO}), 3.19 (s, 3H, CH_3–N). $^{13}C\{^1H\}$ NMR (101 MHz, CD_2Cl_2): δ 159.22 (C–O), 157.62 (C_{imi}–Ni), 127.77 (C_{PhO}–N), 127.62 (C_{PhO}–H), 124.06 (C_{imi}–H), 122.42 (C_{PhO}–H), 118.23 (C_{imi}–H), 117.57 (C_{PhO}–H), 113.64 (C_{PhO}–H), 37.01 (CH_3–N). HR-MS (ESI): calcd for $C_{20}H_{17}N_4NaNiO_2$ $[M + Na]^+$ m/z = 426.0597 (found 426.0603). Anal. calcd for $C_{20}H_{17}N_4NiO_2$ (404.08): C, 59.45; H, 4.24; N, 13.87. Found: C, 59.81; H, 3.95; N, 14.01.

Synthesis of *cis*-[Ni(trz^{Bu}^OPh(Me)$_2$)$_2$] (6a)

According to the general procedure, triazolium salt **5a** (200 mg, 0.5 mmol), K_2CO_3 (140 mg, 1.0 mmol) and $NiCl_2$ (42 mg, 0.3 mmol) were suspended in dry MeCN (10 mL). The residual powder was purified by column chromatography (Al_2O_3 basic; CH_3CN/CH_2Cl_2 1 : 1) to afford complex **6a** as a bright yellow crystalline solid (100 mg, 71%).^{1}H NMR (400 MHz, CD_2Cl_2): δ 7.27 (s, 1H, H_{Ph}), 6.82 (s, 1H, H_{Ph}), 3.88 (s, 3H, N–CH_3), 2.18 (s, 3H, CH_3), 2.16 (s, 3H, CH_3), 1.91 (s, b, 1H, CH–Pr), 1.81 (s, b, 1H, CH–Pr), 1.56 (s, b, 1H,CH–Et), 1.43 (s, b, 1H, CH–Et), 1.23–1.14 (m, 2H, CH_2–CH_3), 0.66 (t, J = 4 Hz, CH_3). $^{13}C\{^1H\}$ NMR (101 MHz, CD_2Cl_2): δ 156.33 (C–O), 146.28 (C_{trz}–Ph), 142.68 (C_{trz}–Ni), 131.26 (C_{Ph}–H), 130.67 (C_{Ph}–H), 126.21 (C_{PhO}–N), 121.10 (C_{Ph}–H), 117.13 (C_{Ph}–H), 36.47 (CH_3–N), 32.25 (CH_2–Pr), 24.99 (CH_3), 22.98 (CH_2–Et), 20.74 (CH_3), 17.15 (CH_2–CH_3), 13.72 (CH_3). HR-MS (ESI): calcd for $C_{30}H_{40}N_6NiO_2$ $[M + H]^+$ m/z = 575.2639 (found 575.2638). Anal. calcd for $C_{30}H_{24}N_6NiO_2$ (575.38): C, 62.62; H, 7.01; N, 14.61. Found: C, 62.33; H, 7.12; N, 14.54.

Synthesis of *cis*-[Ni(trz^{Bu}^OPh(tBu)$_2$)$_2$] (6b)

Triazolium salt **5b** (300 mg, 0.61 mmol) was dissolved in 10 mL of THF in a Schlenk tube under inert atmosphere and the solution stirred at −78 °C for 5 min. After that time a 2.5 M solution of BuLi in hexane (0.56 mL, 1.40 mmol) was added, and the reaction mixture stirred for 30 min and then cannulated to another Schlenk tube containing $NiCl_2$ (44 mg, 0.34 mmol) suspended in 5 ml of THF. The reaction mixture was stirred for 16 h at room temperature. After that time, the reaction was quenched, and the solvent removed under vacuum. DCM (30 mL) was added to the solid and the suspension was filtrated through a short Celite pad. The solvent was removed to leave a bright orange solid, which was then purified by column chromatography (basic Alox CH_3CN/DCM 1 : 5) to obtain complex **6b** as a dark yellow powder (280 mg, 62%). ^{1}H NMR (400 MHz, CD_2Cl_2): δ 7.44 (d, J = 2.1 Hz, 1H, H_{PhO}), 7.30 (d, J = 2.1 Hz, 1H, H_{PhO}), 4.23 (s, 3H, CH_3), 2.34 (t, J = 6.0 Hz, 2H, CH_2–C_3H_7), 1.67 (s, b, 1H, CH_2–C_2H_5), 1.47 (s, b, 1H, CH_2–C_2H_5), 1.37–1.29 (m, 10H, $(CH_3)_3$–C + CH_2–CH_3), 1.28–1.24 (m, 10H, $(CH_3)_3$–C + CH_2–CH_3) 0.76 (t, 3H, J = 6.0 Hz, CH_3). $^{13}C\{^1H\}$ NMR (100 MHz, CD_2Cl_2): δ 154.24 (C–O), 145.50 (C_{Ph}), 141.85 (C_{Ph}), 138.89 (C_{Trz}–Ni), 128.53 (C_{Ph}–H), 126.22 (C_{Ph}–N), 122.42 (C_{Trz}–Bu), 121.58 (C_{Ph}–H), 38.89 ($C(CH)_3$), 36.19 ($C(CH)_3$), 34.73 (CH_3–N), 31.70 (CH_3), 29.23 (CH_3), 28.52 (CH_2–C_3H_7), 23.49 (CH_2–C_2H_5), 23.25 (CH_2–CH_3), 13.77 (–CH_3). HR-MS (ESI): calcd for $C_{42}H_{64}N_6NiO_2$ $[M + H]^+$ m/z = 743.4517 (found 743.4495). Anal. calcd for $C_{42}H_{64}N_6NiO_2$ (743.70): C, 67.83; H, 8.67; N, 11.30. Found: C, 67.76; H, 8.88; N, 11.35.

Crystal structure determinations. Suitable crystals of **3a–c**, **4** and **6a-b** were mounted in air at ambient conditions and measured on an Oxford Diffraction SuperNova area–detector diffractometer at T = 173(2) K by using mirror optics monochromated $Mo_{K\alpha}$ radiation (λ = 0.71073 Å) and Al filtered.[64] Data reduction was performed by using the CrysAlisPro

program.[65] The intensities were corrected for Lorentz and polarization effects, and an absorption correction based on the multi–scan method by using SCALE3 ABSPACK in CrysAlisPro was applied. The structures were solved by direct methods by using SHELXT, and all non–hydrogen atoms were refined anisotropically.[66] All hydrogen atoms were placed in geometrically calculated positions and refined by using a riding model with each hydrogen atom assigned a fixed isotropic displacement parameter (1.2*U*eq of its parent atom, 1.5*U*eq for the methyl groups). Structures were refined on F^2 by using full–matrix least–squares procedures. The weighting schemes were based on counting statistics and included a factor to downweight the intense reflections. All calculations were performed by using the SHELXL-2014 program.[67] Further crystallographic details are compiled in Tables S1–6 in the ESI.† Crystallographic data for all structures have been deposited with the Cambridge Crystallographic Data Centre (CCDC) as supplementary publication numbers 2004183 (**3a**), 2004182 (**3b**), 2004184 (**3c**), and 2004181 (**4**), 2050371 (**6a**), 2050372 (**6b**).†

Conflicts of interest

The authors declare no competing financial interest.

Acknowledgements

We thank the Swiss National Science Foundation (200020_182663 and 200020_172507), the Marie Sklodowska Curie ITN NoNoMeCat (grant 675020-MSCA-ITN-2015-ETN), and the European Research Council (CoG 615653) for generous financial support of this work. We also thank the crystallography service unit of the University of Bern for analytical work (funded through SNSF R'equip 206021_128724). A.R. acknowledges support from the Ministry of Science and Higher Education of the Russian Federation.

Notes and references

1 M. Aresta, *Carbon Dioxide as Chemical Feedstock*, Wiley-VCH Verlag GmbH & Co. KGaA, 2010, Weinheim, Germany.
2 C. Costentin, M. Robert and J.-M. Savéant, *Chem. Soc. Rev.*, 2013, **42**, 2423–2436.
3 A. M. Appel, J. E. Bercaw, A. B. Bocarsly, H. Dobbek, D. L. DuBois, M. Dupuis, J. G. Ferry, E. Fujita, R. Hille, P. J. A. Kenis, C. A. Kerfeld, R. H. Morris, C. H. F. Peden, A. R. Portis, S. W. Ragsdale, T. B. Rauchfuss, J. N. H. Reek, L. C. Seefeldt, R. K. Thauer and G. L. Waldrop, *Chem. Rev.*, 2013, **113**, 6621–6658.
4 M. Mikkelsen, M. Jørgensen and F. C. Krebs, *Energy Environ. Sci.*, 2010, **3**, 43–81.
5 M. Aresta, A. Dibenedetto and A. Angelini, *Chem. Rev.*, 2014, **114**(3), 1709–1742.
6 W. Tu, Y. Zhou and Z. Zou, *Adv. Mater.*, 2014, **26**, 4607–4626.
7 J. P. Jones, G. K. S. Prakash and G. A. Olah, *Isr. J. Chem.*, 2014, **54**, 1451–1466.
8 Y. Matsubara, D. C. Grills and Y. Kuwahara, *ACS Catal.*, 2015, **5**, 6440–6452.
9 X. Min and M. W. Kanan, *J. Am. Chem. Soc.*, 2015, **137**, 4701–4708.
10 M. Rahaman, A. Dutta and P. Broekmann, *ChemSusChem*, 2017, **10**, 1733–1741.
11 G. Reitz, *J. Electrochem. Soc.*, 1985, **132**, 8C.
12 K. P. Kuhl, T. Hatsukade, E. R. Cave, D. N. Abram, J. Kibsgaard and T. F. Jaramillo, *J. Am. Chem. Soc.*, 2014, **136**, 14107–14113.
13 D. Ren, Y. Deng, A. D. Handoko, C. S. Chen, S. Malkhandi and B. S. Yeo, *ACS Catal.*, 2015, **5**, 2814–2821.
14 M. Rahaman, A. Dutta, A. Zanetti and P. Broekmann, *ACS Catal.*, 2017, **7**, 7946–7956.
15 Y. Hori, K. Kikuchi and S. Suzuki, *Chem. Lett.*, 1985, **14**, 1695–1698.
16 A. Dutta, C. E. Morstein, M. Rahaman, A. Cedeño López and P. Broekmann, *ACS Catal.*, 2018, **8**, 8357–8368.
17 A. S. Varela, W. Ju, A. Bagger, P. Franco, J. Rossmeisl and P. Strasser, *ACS Catal.*, 2019, **9**, 7270–7284.
18 B. Plietker, *Iron Catalysis in Organic Chemistry: Reactions and Applications*, 2008, John Wiley & Sons, NY.
19 R. M. Bullock, *Catalysis without precious metals*, 2011, John Wiley & Sons, NY.
20 N. Elgrishi, M. B. Chambers, X. Wang and M. Fontecave, *Chem. Soc. Rev.*, 2017, **46**, 761–796.
21 (*a*) I. Bhugun, D. Lexa and J.-M. Savéant, *J. Am. Chem. Soc.*, 1996, **118**, 1769–1776; (*b*) C. Costentin, S. Drouet, M. Robert and J.-M. Savéant, *Science*, 2012, **338**, 90–94.
22 M. Stanbury, J. D. Compain and S. Chardon-Noblat, *Coord. Chem. Rev.*, 2018, **361**, 120–137.
23 J. Gu, C. S. Hsu, L. Bai, H. M. Chen and X. Hu, *Science*, 2019, **364**, 1091–1094.
24 Y. Sakaguchi, A. Call, M. Cibian, K. Yamauchi and K. Sakai, *Chem. Commun.*, 2019, **55**, 8552–8555.
25 C. Steinlechner, A. F. Roesel, E. Oberem, A. Päpcke, N. Rockstroh, F. Gloaguen, S. Lochbrunner, R. Ludwig, A. Spannenberg, H. Junge, R. Francke and M. Beller, *ACS Catal.*, 2019, **9**, 2091–2100.
26 Notable exceptions: (*a*) H. Rao, L. C. Schmidt, J. Bonin and M. Robert, *Nature*, 2017, **548**, 74–77; (*b*) S. Roy, B. Sharma, J. Pécaut, P. Simon, M. Fontecave, P. D. Tran, E. Derat and V. Artero, *J. Am. Chem. Soc.*, 2017, **139**, 3685–3696.
27 For the use of CO as valuable product, see: T. Haas, R. Krause, R. Weber, M. Demler and G. Schmid, *Nat. Catal.*, 2018, **1**, 32–39.
28 For a recent overview, see: J.-W. Wang, W.-J. Liu, D.-C. Zhong and T.-B. Lu, *Coord. Chem. Rev.*, 2019, **378**, 237–261.
29 M. Beley, J. P. Collin, R. Ruppert and J.–P. Sauvage, *J. Chem. Soc., Chem. Commun.*, 1984, 1315–1316.
30 M. Beley, J. P. Collin, R. Ruppert and J.–P. Sauvage, *J. Am. Chem. Soc.*, 1986, **108**, 7461–7467.

31 J. P. Collin, A. Jouaiti and J.–P. Sauvage, *Inorg. Chem.*, 1988, **27**, 1986–1990.
32 T. Fogeron, T. K. Todorova, J.–P. Porcher, M. Gomez-Mingot, L.–M. Chamoreau, C. Mellot-Draznieks, Y. Li and M. Fontecave, *ACS Catal.*, 2018, **8**, 2030–2038.
33 J. D. Froehlich and C. P. Kubiak, *Inorg. Chem.*, 2012, **51**, 3932–3934.
34 C. A. Huff and M. S. Sanford, *ACS Catal.*, 2013, **3**, 2412–2416.
35 F. Bertini, M. Glatz, N. Gorgas, B. Stöger, M. Peruzzini, L. F. Veiros, K. Kirchner and L. Gonsalvi, *Chem. Sci.*, 2017, **8**, 5024–5029.
36 F. Bertini, M. Glatz, B. Stöger, M. Peruzzini, L. F. Veiros, K. Kirchner and L. Gonsalvi, *ACS Catal.*, 2019, **9**, 632–639.
37 K. F. Donnelly, A. Petronilho and M. Albrecht, *Chem. Commun.*, 2013, **49**, 1145–1159.
38 A. Vivancos, C. Segarra and M. Albrecht, *Chem. Rev.*, 2018, **118**, 9493–9586.
39 D. Bourissou, O. Guerret, F. P. Gabbaï and G. Bertrand, *Chem. Rev.*, 2000, **100**, 39–92.
40 W. A. Herrmann, *Angew. Chem., Int. Ed.*, 2002, **41**, 1290–1309.
41 F. E. Hahn and M. C. Jahnke, *Angew. Chem., Int. Ed.*, 2008, **47**, 3112–3172.
42 Y. Wei, A. Petronilho, H. Mueller-Bunz and M. Albrecht, *Organometallics*, 2014, **33**, 5834–5844.
43 S. Hameury, P. de Frèmont and P. Braunstein, *Chem. Soc. Rev.*, 2017, **46**, 632–733.
44 L. Yang, D. R. Powell and R. P. Houser, *Dalton Trans.*, 2007, **9**, 955–964.
45 C. J. Johnson and M. Albrecht, *Organometallics*, 2017, **36**, 2902–2913.
46 J. M. Smieja, M. D. Sampson, K. A. Grice, E. E. Benson, J. D. Froehlich and C. P. Kubiak, *Inorg. Chem.*, 2013, **52**, 2484–2491.
47 C. Costentin, S. Drouet, M. Robert and J.–M. Savéant, *J. Am. Chem. Soc.*, 2012, **134**, 11235–11242.
48 Chronoamperometric measurements indicate a gradual decrease of the catalytic current when performing measurements over time periods larger than 10 min, which complicated the determination of catalytic efficiency, see ESI for details.†
49 A. V. Rudnev, U. E. Zhumaev, A. Kuzume, S. Vesztergom, J. Furrer, P. Broekmann and T. Wandlowski, *Electrochim. Acta*, 2016, **189**, 38–44.
50 Y. Hori, H. Wakebe, T. Tsukamoto and O. Koga, *Electrochim. Acta*, 1994, **39**, 1833–1839.
51 P. Hemberger, G. da Silva, A. J. Trevitt, T. Gerbera and A. Bodi, *Phys. Chem. Chem. Phys.*, 2015, **17**, 30076–30083.
52 E. R. Altwicker, *Chem. Rev.*, 1967, **67**, 475–531.
53 C. Gunanathan, Y. Ben-David and D. Milstein, *Science*, 2007, **317**, 790–792.
54 S. Rösler, J. Obenauf and R. Kempe, *J. Am. Chem. Soc.*, 2015, **137**, 7998–8001.
55 A. Mukherjee and D. Milstein, *ACS Catal.*, 2018, **8**, 11435–11469.
56 M. Fujihira, Y. Hirata and K. Suga, *J. Electroanal. Chem.*, 1990, **292**, 199–215.
57 J. A. Keith, K. A. Grice, C. P. Kubiak and E. A. Carter, *J. Am. Chem. Soc.*, 2013, **135**, 15823–15829.
58 N. J. Firet and W. A. Smith, *ACS Catal.*, 2017, **7**, 606–612.
59 L. Zhang, Z.–J. Zhao and J. Gong, *Angew. Chem., Int. Ed.*, 2017, **56**, 11326–11353.
60 J. Song, E. L. Klein, F. Neese and Y. Shengfa, *Inorg. Chem.*, 2014, **53**, 7500–7507.
61 F. Dulong, O. Bathily, P. Thuery, M. Ephritikhine and T. Cantat, *Dalton Trans.*, 2012, **41**, 11980–11983.
62 M. Liu, M. Nieger, E. G. Habner and A. Schmidt, *Chem. – Eur. J.*, 2016, **22**, 5416–5424.
63 Y. N. Kotovshchikov, G. V. Latyshev, M. A. Navasardyan, D. A. Erzunov, I. P. Beletskaya and N. V. Lukashev, *Org. Lett.*, 2018, **20**(15), 4467–4470.
64 Oxford Diffraction, *CrysAlisPro (Version 1.171.38.41)*, Oxford Diffraction Ltd., Yarnton, Oxfordshire, UK, 2010.
65 P. Macchi, H. B. Bürgi, A. S. Chimpri, J. Hauser and Z. Gál, *J. Appl. Crystallogr.*, 2011, **44**, 763–771.
66 G. M. Sheldrick, *Acta Crystallogr., Sect. A: Found. Adv.*, 2015, **A71**, 3–8.
67 G. M. Sheldrick, *Acta Crystallogr., Sect. C: Struct. Chem.*, 2015, **C71**, 3–8.